J|A|C|S
ARTICLES
Published on Web 07/15/2006

Ferromagnetic Coupling in Hexanuclear Gadolinium Clusters

Lucas E. Sweet, Lindsay E. Roy, Fanqin Meng, and Timothy Hughbanks*

Contribution from the Department of Chemistry, Texas A&M University, P.O. Box 30012, College Station, Texas 77842-3012

Received March 29, 2006; E-mail: trh@mail.chem.tamu.edu

Abstract: The magnetic susceptibilities of hexanuclear gadolinium clusters in the compounds $Gd(Gd_6ZI_{12})$ (Z = Co, Fe, or Mn) and $CsGd(Gd_6CoI_{12})_2$ are reported and subjected to theoretical analysis with the help of density functional theory (DFT) computations. The single-crystal structure of $Gd(Gd_6CoI_{12})$ is reported here as well. We find that the compound with a closed shell of cluster bonding electrons, $Gd(Gd_6CoI_{12})$, exhibits the effects of antiferromagnetic coupling over the entire range of temperatures measured (4−300 K). Clusters with unpaired, delocalized cluster bonding electrons (CBEs) exhibit enhanced susceptibilities consistent with strong ferromagnetic coupling, except at lower temperatures (less than 30 K) where intercluster antiferromagnetic coupling suppresses the susceptibilities. The presence of two unpaired CBEs, as in $[Gd_6MnI_{12}]^{3-}$, yields stronger coupling than when just one unpaired CBE is present, as in $[Gd_6FeI_{12}]^{3-}$ or $[Gd_6CoI_{12}]^{2-}$. DFT calculations on model molecular systems, $[Gd_6CoI_{12}](OPH_3)_6$ and $[Gd_6CoI_{12}]_2(OPH_3)_{10}$, indicate that the delocalized cluster bonding electrons are highly effective at mediating intracluster ferromagnetic exchange coupling between the Gd atom $4f^7$ moments and that intercluster coupling is expected to be antiferromagnetic. The DFT calculations were used to calculate the relative energies of various $4f^7$ spin patterns and form the basis for construction of a simple spin Hamiltonian describing the coupling within the $[Gd_6CoI_{12}]$ cluster.

Introduction

High-spin molecules, especially those which behave as single molecule magnets (SMMs), continue to be of intense interest.[1−9] It was not until recently that research describing single molecule magnets containing lanthanides was published. Ishikawa et al. have shown that lanthanide-based molecules can exhibit marked SMM behavior, the origin of which is different from that of transition metal based molecules.[10] SMM behavior has also been observed in 4f−3d heterometallic $[Tb^{III}_2Cu^{II}_2]$[11] and $[Dy^{III}_2Cu^{II}]$[12] complexes. Lanthanide-containing molecules are promising because they have the potential to yield a large number of unpaired electrons and, for those with orbitally degenerate spin−orbit states, are often split by the crystal field to give ground states with substantial magnetic anisotropy.[10,13,14] Most of the work in this field has been on single lanthanide atom molecules and/or compounds containing lanthanides in their 3+ oxidation state.[15]

The sizable intraatomic exchange energy involving electrons in the valence 5d/6s and corelike 4f orbitals in Ln atoms provides a mechanism for coupling the 4f orbitals moments on two or more lanthanide atoms—via electrons in the bonding orbitals. Since the 4f orbitals are highly contracted, their direct involvement in Ln-ligand bonding is very limited, and magnetic coupling via Ln−ligand−Ln superexchange is very small. However, if there are unpaired electrons with significant 5d/6s character delocalized over lanthanide centers, electrons localized in the 4f orbitals can couple strongly. This interaction is therefore maximized when the lanthanides are reduced below the typical 3+ oxidation state.

In this paper, we investigate the series of compounds $Gd(Gd_6ZI_{12})$ (Z = Co, Fe, or Mn)[16] and $CsGd(Gd_6CoI_{12})_2$, which are comprised of reduced gadolinium clusters that are cross-linked by iodide bridges. These compounds provide a series of systems in which the Z-centered hexanuclear gadolinium clusters

(1) Oshio, H.; Hoshino, N.; Ito, T.; Nakano, M. *J. Am. Chem. Soc.* **2004**, *126*, 8805−8812.
(2) Moragues-Canovas, M.; Helliwell, M.; Ricard, L.; Riviere, E.; Wernsdorfer, W.; Brechin, E.; Mallah, T. *Eur. J. Inorg. Chem.* **2004**, 2219−2222.
(3) Murugesu, M.; Habrych, M.; Wernsdorfer, W.; Abboud, K. A.; Christou, G. *J. Am. Chem. Soc.* **2004**, *126*, 4766−4767.
(4) Murugesu, M.; Raftery, J.; Wernsdorfer, W.; Christou, G.; Brechin, E. K. *Inorg. Chem.* **2004**, *43*, 4203−4209.
(5) Takagami, N.; Ishida, T.; Nogami, T. *Bull. Chem. Soc. Jpn.* **2004**, *77*, 1125−1134.
(6) Tasiopoulos, A. J.; Vinslava, A.; Wernsdorfer, W.; Abboud, K. A.; Christou, G. *Angew. Chem., Int. Ed.* **2004**, *43*, 2117−2121.
(7) Cornia, A.; Fabretti, A. C.; Garrisi, P.; Mortalo, C.; Bonacchi, D.; Sessoli, R.; Sorace, L.; Barra, A. L.; Wernsdorfer, W. *J. Magn. Magn. Mater.* **2004**, *272−276*, E749−E751.
(8) Bian, G.-Q.; Kuroda-Sowa, T.; Konaka, H.; Hatano, M.; Maekawa, M.; Munakata, M.; Miyasaka, H.; Yamashita, M. *Inorg. Chem.* **2004**, *43*, 4790−4792.
(9) Zhao, H.; Berlinguette, C. P.; Bacsa, J.; Prosvirin, A. V.; Bera, J. K.; Tichy, S. E.; Schelter, E. J.; Dunbar, K. R. *Inorg. Chem.* **2004**, *43*, 1359−1369.
(10) Ishikawa, N.; Sugita, M.; Ishikawa, T.; Koshihara, S.; Kaizu, Y. *J. Phys. Chem. B* **2004**, *108*, 11265−11271.
(11) Osa, S.; Kido, T.; Matsumoto, N.; Re, N.; Pochaba, A.; Mrozinski, J. *J. Am. Chem. Soc.* **2004**, *126*, 420−421.
(12) Mori, F.; Nyui, T.; Ishida, T.; Nogami, T.; Choi, K.-Y.; Nojiri, H. *J. Am. Chem. Soc.* **2006**, *128*, 1440−1441.
(13) Ishikawa, N.; Sugita, M.; Ishikawa, T.; Koshihara, S.-Y.; Kaizu, Y. *J. Am. Chem. Soc.* **2003**, *125*, 8694−8695.
(14) Ishikawa, N.; Otsuka, S.; Kaizu, Y. *Angew. Chem., Int. Ed.* **2005**, *44*, 731−33.
(15) Tang, J.; Hewitt, I.; Madhu, N. T.; Chastanet, G.; Wernsdorfer, W.; Anson, C. E.; Benelli, C.; Sessoli, R.; and Powell, A. K. *Angew. Chem.* **2006**, *45*, 1729−33.
(16) Hughbanks, T.; Corbett, J. D. *Inorg. Chem.* **1988**, *27*, 2022−6.

exhibit varying electron counts and allow us to investigate the effect that unpaired delocalized electrons have on magnetic coupling within the clusters. In the temperature-dependent magnetic susceptibility measurements and theoretical calculations reported here, we propose an exchange mechanism that explains the magnetic properties of compounds that contain Gd_6ZI_{12} clusters.

Experimental Section

Materials and Methods. All compounds were manipulated in a nitrogen atmosphere glovebox or on high-vacuum lines. Reactions were carried out in Nb tubes, which were welded closed under a partial pressure of Ar and sealed in evacuated silica jackets. GdI_3 was synthesized by reaction of Gd metal turnings with HgI_2, as described in the literature, and sublimed at least three times.[17,18] The transition metal iodides were synthesized from the elements and sublimed—FeI_2 under dynamic vacuum and MnI_2 and CoI_2 under static vacuum. CsI (Aesar 99%) was sublimed under dynamic vacuum and stored in ampules until use. Gadolinium metal ingots were acquired from Stanford Materials (99.95% REM) and the Ames Laboratory (99.999%, including nonmetals). Turnings of these metals were obtained by drilling the ingots (in a glovebox) using a tungsten carbide drill bit and then collected and stored in evacuated ampules until their use.

Synthesis. $Gd[Gd_6ZI_{12}]$ (Z = Mn, Fe, or Co) were prepared in reactions loaded with stoichiometric proportions of GdI_3, ZI_2 (Z = Mn, Fe, Co), and Gd metal turnings and heated in Nb tubes to 850 °C for 16 days, as described previously.[16] $CsGd[Gd_6CoI_{12}]_2$ was synthesized by mixing CsI, GdI_3, CoI_2, and Gd metal turnings in a 3:19:6:23 ratio and heating to 750 °C for 500 h, followed by slow cooling (4.5 °C/h) to 300 °C (reference to be published). To minimize contamination of samples by ferromagnetic impurities, Teflon or Teflon-coated utensils were used when handling the products.

X-ray Diffraction Studies. The products were identified by use of X-ray powder diffraction. The purity of the compounds was evaluated by comparison of their X-ray powder patterns with those calculated on the basis of reported structures or single-crystal data. A Bruker AXS D8 powder X-ray diffractometer equipped with a graphite-monochromated Cu Kα X-ray source was used with an airtight sample holder to obtain powder diffraction patterns of the samples. Using the program Powder Cell for Windows,[19] diffraction peaks from the samples were matched with the calculated diffraction peaks from the corresponding crystal structures. The desired cluster compounds were identified as the major phases, with GdOI identifiable as a side product (~1−5%).

X-ray diffraction data were collected on a single crystal of $Gd(Gd_6CoI_{12})$, using a Bruker SMART 1000 CCD X-ray diffractometer equipped with graphite-monochromated Mo Kα radiation ($\lambda = 0.710\ 73$ Å). The crystal was mounted on nylon loops using Apeizon N grease and then placed in a N_2 stream at 110 K for data collection. Frame data was indexed using SMART software,[20] and the peak intensities were integrated using SAINT software.[21] Absorption corrections were made using SADABS software.[22] The SHELXTL version 6.12 software package[23] was used as an interface to the SHELX-97 suite of programs,[24] which was used to implement structure solutions by direct methods and full-matrix least-squares structural refinements on F^2.

Magnetic Measurements. Magnetic measurements were performed with a Quantum Design SQUID magnetometer MPMSXL on polycrystalline samples of $Gd[Gd_6MnI_{12}]$, $Gd[Gd_6FeI_{12}]$, $Gd[Gd_6CoI_{12}]$, and $CsGd(Gd_6CoI_{12})_2$. Temperature-dependent magnetization data were collected at 2−5 K intervals from 2 to 300 K in applied fields of 0.1, 0.5, 1.0, 2.0, 3.0, and 3.5 T. All data were corrected for the sample holder contribution and for the intrinsic diamagnetic contributions after the measurements.[25]

Computational Studies. The electronic structures of models for $Gd[Gd_6ZI_{12}]$ (Z = Mn, Fe, Co) were investigated by use of density functional theory (DFT) with the Becke exchange functional and the Lee−Yang−Parr correlation functional (BLYP).[26,27] All calculations presented here were performed using the DMol^3 program from the Cerius2 suite of programs using the double numerical basis including d-polarization functions (DND).[28−30] A small frozen-core (1s2s2p3s3p3d) and (1s2s2p) effective potential was used for Gd and Co, respectively. A large frozen-core (1s2s2p3s3p3d4s4p4d4f) effective potential was used for I. All calculations included scalar relativistic effects and open-shell configurations.

Structural parameters for the heavy elements (Gd, I, and Z) were taken from the X-ray crystallographic data for the condensed cluster phase $Gd[Gd_6ZI_{12}]$, as described below. In the construction of the model compounds, phosphine oxide ligands, OPH_3, were used to "cap-off" the terminal positions of the Gd_6ZI_{12} cluster; partial geometry optimizations for the positions of the phosphine oxides were performed using an analogous yttrium model system. All calculations of competing magnetic states were conducted using a common geometry. The convergence criterion for the energy was set at 10^{-6} au.

Theoretical Background

The 4f orbitals on lanthanide atoms are highly contracted, and their participation in Ln−ligand superexchange coupling is effectively precluded. However, a substantial *intraatomic* exchange interaction between 4f electrons and valence 5d and 6s electrons is present. Atomic spectral data for Gd ($[Xe]4f^75d^16s^2$)[13] show a large energetic cost of "flipping" the $4f^7$ spin in opposition to the 5d electron ($E(^9D) - E(^7D) = 0.793$ eV; computed to be 0.706 eV in our calculations).[31,32] The $4f^7$-exchange field can be viewed as a contact interaction that exerts its direct influence only on orbitals centered on the gadolinium atom because only the valence 5d and 6s electrons significantly penetrate the atomic core, where they experience the effect of this exchange field. The more contracted 5d orbitals penetrate to a greater extent than the 6s orbital, and consequently the 5d electrons experience greater exchange interaction with the $4f^7$ core.

Figure 1 illustrates how the potential from the $4f^7$ core affects electrons that reside in with 5d and 6s character for the Gd atom. At the left side of this figure, we depict an "unperturbed" system wherein the valence d electron experiences an average exchange potential from the half-filled 4f shell, so the d electron has no preferred spin orientation. Upon application of the exchange field, the spin aligned with (against) the 4f spins is stabilized (destabilized) by an energy δ. For a Gd atom, 2δ is just the difference between the ^9D ground state and the first excited state, ^7D. These exchange interactions are intrinsically "ferromagnetic", favoring parallel alignment of the 4f and 5d spins.

(17) Corbett, J. D. *Inorg. Synth.* **1983**, *22*, 31−6.
(18) Corbett, J. D. *Inorg. Synth.* **1983**, *22*, 15−22.
(19) Kraus, W.; Nolze, G. *POWDER CELL-V2.4 Program for viewing powder patterns*; Federal Institute for Materials Research and Testing: Berlin, Germany, 2000.
(20) *SMART-V5.625 Program for Data Collection on Area Detectors*; Bruker AXS Inc.: Madison, WI, 2001.
(21) *SAINT-V6.63 Program for Reduction of Area Detector Data*; Bruker AXS Inc.: Madison, WI, 2001.
(22) Sheldrick, G. M. *SADABS-V 2.03 Program for Absorption Correction of Area Detector Frames*; Bruker AXS Inc.: Madison, WI, 2001.
(23) *SHELXTL-V6.12 (PC-version) Program for Structure Solution, Refinement and Presentation*; Bruker AXS Inc.: Madison, WI, 2000.
(24) Sheldrick, G. *SHELXL-97 Program for Crystal Structure Refinement*; Institüt für Anorganische Chemie der Universität: Gottingen, Germany, 1997.
(25) Kahn, O. *Molecular Magnetism*; VCH: New York, 1993.
(26) Becke, A. D. *Phys. Rev. A: At. Mol. Opt. Phys.* **1988**, *38*, 3098−100.
(27) Lee, C.; Yang, W.; Parr, R. G. *Phys. Rev. B: Condens. Matter* **1988**, *37*, 785−9.
(28) Delley, B. *J. Chem. Phys.* **1990**, *92*, 508−17.
(29) Delley, B. *Int. J. Quantum Chem.* **1998**, *69*, 423−33.
(30) Delley, B. *J. Chem. Phys.* **2000**, *113*, 7756−64.
(31) Martin, W. C.; R. Z.; Hagan, L. *Natl. Stand. Ref. Data Ser., Natl. Bur. Stand.* **1978**, *60*.
(32) Roy, L. E.; Hughbanks, T. *Mater. Res. Soc. Symp. Proc.* **2002**, *755*, 25−30.

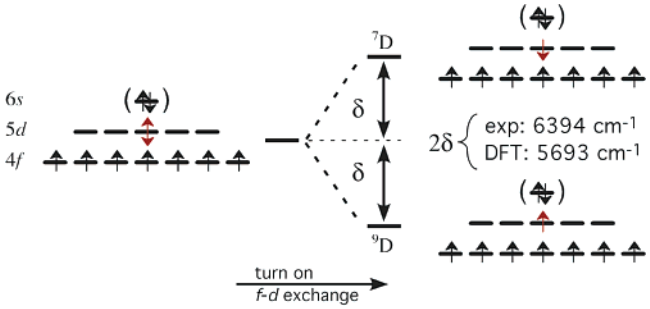

Figure 1. Electronic splitting of the Gd atom as a function of 4f−5d exchange perturbation.

Before turning our attention to the manner in which magnetic moments in polynuclear gadolinium systems are coupled, let us first consider the general formalism of magnetic coupling. The Heisenberg−Dirac−Van Vleck (HDVV) spin Hamiltonian is used to describe the exchange interaction between two paramagnetic centers:[33−35]

$$\hat{H} = -J_{ij}\hat{S}_i\hat{S}_j \tag{1}$$

Here J_{ij} is the so-called magnetic coupling constant describing the spin exchange between different states and S_i and S_j are the total spin operators for atoms i and j, respectively. The sign of the magnetic coupling constant is such that J_{ij} is positive for ferromagnetic coupling. In the case where $S = 1/2$, two magnetic centers are coupled.

$$J = E(\mathrm{S}) - E(\mathrm{T}) \tag{2}$$

In principle, the calculation of a magnetic coupling constant involves the computation of the energy of high-spin and low-spin states, but because density functional theory (DFT) is generally implemented as a single-determinant method, pure spin eigenfunctions are excluded for any but the highest spin states. For the high spin state $|S\ M_s\rangle$, spin contamination is limited to the small spin contamination inherent to the use of an open-shell (spin-polarized) calculation. Lower spin state eigenfunctions are expressed as linear combinations of Slater determinants and therefore are not amenable to direct calculation in the usual implementation of spin DFT (SDFT). Noodleman and others proposed an alternative approach, in which spin-polarized functions are evaluated within the density functional formalism and the expectation value(s) for broken symmetry (BS) solution(s) are used in calculating the energy of the low-spin state(s).[36−38]

We have shown in previous work that exchange coupling in gadolinium-containing systems is effectively accounted for in this approach.[32,39,40] As an instructive example, consider a dinuclear gadolinium system (two magnetic centers $S_1 = S_2 = 7/2$). SDFT is first used to calculate the energy of $|\uparrow_7,\uparrow_7\rangle$ and $|\uparrow_7,\downarrow_7\rangle$, where $|\uparrow_7,\uparrow_7\rangle$ represents a state with all seven of the f electrons on both Gd atoms are spin up and $|\uparrow_7,\downarrow_7\rangle$ represents a determinant where all seven f electrons on one Gd atom are spin up and all seven on the other Gd atom are spin down. The "energy" of the BS ($|\uparrow_7,\downarrow_7\rangle$) determinant is then equal to an appropriate weighted average of the energies of pure spin multiplets (pure spin determinants with $S = 0, 1, ..., 7$ and $M_s = 0$), and J can be obtained through the equation

$$\frac{49}{2}J = E_{|\uparrow_7,\downarrow_7\rangle} - E_{|\uparrow_7,\uparrow_7\rangle} \tag{3}$$

(33) Heisenberg, W. *Z. Phys.* **1928**, *49*, 619−36.
(34) Dirac, P. A. M. *Proc. R. Soc. (London)* **1929**, *A123*, 714−33.
(35) Van Vleck, J. H. *The Theory of Electric and Magnetic Susceptibilities*; Oxford: Oxford, U.K., 1932.
(36) Noodleman, L. *J. Chem. Phys.* **1981**, *74*, 5737−43.
(37) Caballol, R.; Castell, O.; Illas, F.; de Moreira, I.; Malrieu, J. P. *J. Phys. Chem. A* **1997**, *101*, 7860−7866.
(38) Illas, F.; De P. R. Moreira, I.; Bofill, J. M.; Filatov, M. *Phys. Rev. B: Condens. Matter* **2004**, *70*, 132414/1−132414/4.

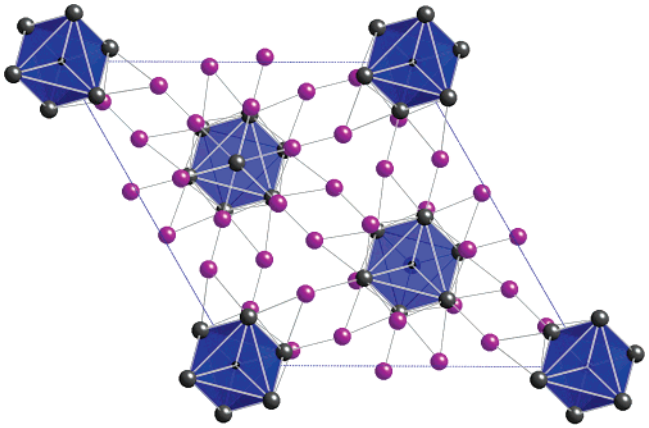

Figure 2. *c*-axis projection of $Gd(Gd_6CoI_{12})$ ($R\bar{3}$).

To qualitatively ascertain the structural and electronic characteristics that determine whether a particular system will exhibit ferro- or antiferromagnetic coupling, it is often useful to examine the characteristics of the broken symmetry solution, $|\uparrow_7,\downarrow_7\rangle$, though it does not actually represent any (single) spin eigenfunction ($|\downarrow_7,\uparrow_7\rangle$ makes an equal contribution to the $S = 0$ state, for example). Whatever factors one can identify that tend to (de)stabilize $|\uparrow_7,\downarrow_7\rangle$ versus $|\uparrow_7,\uparrow_7\rangle$ (a true spin eigenfunction) will proportionately affect the (de)stabilization of the true low-spin eigenfunction. In the same spirit, we shall discuss certain characteristics of broken symmetry determinant(s), such as spin-polarization of Gd 6s and 5d electrons induced by the $4f^7$ core electrons, to gain insight into the origin of magnetic coupling in polynuclear clusters.

Results and Discussion

Structures. The rhombohedral $R[R_6ZX_{12}]$ structure ($R\bar{3}$ or $R3$) has been determined for R = Sc, Y, and many of La−Lu, where X = Cl, Br, or I.[16,41−44] Because we focus here on the magnetic properties of Gd-containing clusters, $Gd[Gd_6ZI_{12}]$, we have determined the single-crystal structures, features of which may have an effect on the electronic and magnetic properties. These structures exhibit one crystallographically distinct cluster/cell (Figure 2); all 12 Gd−Gd edges of the cluster are bridged by one of two crystallographically distinct iodide atoms. Six iodine atoms bridge the "waist" edges of each Gd_6 octahedron and simultaneously form exo bonds to metal vertices of adjacent clusters (X^{i-a}). The other six halide atoms bridge Gd−Gd edges at the "top" and "bottom" triangular faces of the Gd_6 trigonal antiprism (I^i). The seventh Gd atom, located midway between the $(Gd_6Z)I_{12}$ clusters along the *c* axis, binds to six I^i atoms that form a trigonal antiprism. Because it does not participate in metal−metal bonding, it can be regarded as Gd^{III} ion. Using the established notation, the structures are thus described as $Gd^{3+}[Gd_6Z(I^i)_6(I^{i-a})_{6/2}(I^{a-i})_{6/2}]^{3-}$. In the centric ($R\bar{3}$) structures, the symmetry of the Gd_6ZI_{12} clusters deviates very slightly from D_{3d} and the departure from octahedral symmetry is small enough that an O_h approximation is still useful in discussing their electronic structure.

(39) Roy, L.; Hughbanks, T. *J. Solid State Chem.* **2003**, *176*, 294−305.
(40) Roy, L. E.; Hughbanks, T. *J. Am. Chem. Soc.* **2006**, *128*, 568−75.
(41) Hwu, S. J.; Corbett, J. D. *J. Solid State Chem.* **1986**, *64*, 331−46.
(42) Dudis, D. S.; Corbett, J. D.; Hwu, S. J. *Inorg. Chem.* **1986**, *25*, 5, 3434−8.
(43) Hughbanks, T.; Rosenthal, G.; Corbett, J. D. *J. Am. Chem. Soc.* **1986**, *108*, 8289−90.
(44) Payne, M. W.; Corbett, J. D. *Inorg. Chem.* **1990**, *29*, 2246−51.

Table 1. Crystallographic Data for $Gd(Gd_6CoI_{12})$

empirical formula	Gd_7CoI_{12}
fw	2682.48 g/mol
temp	110(2) K
cryst system, space group, Z	trigonal, $R\bar{3}$ (No. 148), 3
unit cell dimens a, c	15.412(2), 10.678(2) Å
V	2196.5(6) Å^3
D(calcd)	6.084 g/cm^3
abs coeff	28.800 mm^{-1}
extinctn coeff	$1.54(8) \times 10^{-4}$
final R indices [$I > 2\sigma(I)$]	$R_1 = 0.0247$, $wR_2 = 0.0492$
R indices (all data)	$R_1 = 0.0282$, $wR_2 = 0.0503$

[a] $R_1 = \sum||F_o| - |F_c||/\sum|F_o|$. [b] $wR_2 = \{\sum[w(F_o^2 - F_c^2)^2]/\sum[w(F_o^2)^2]\}^{1/2}$; $w = 1/[\sigma^2(F_o^2) + (0.0166P)^2]$, where $P = (F_o^2 + 2F_c^2)/3$.

Table 2. Atomic Coordinates and Equivalent Isotropic Displacement Parameters (Å$^2 \times 10^3$) for $Gd(Gd_6CoI_{12})$

atom	Wyckoff symbol	x	y	z	U_{eq}[a]
Gd(1)	3*b*	0	0	0.5	9(1)
Gd(2)	18*f*	0.0440(1)	0.1587(1)	0.8586(1)	4(1)
I(1)	18*f*	0.8676(1)	0.0516(1)	0.6599(1)	7(1)
I(2)	18*f*	0.2376(1)	0.3171(1)	0.9947(1)	8(1)
Co(1)	3*a*	0	0	0	3(1)

[a] $U_{eq} = (8\pi^2/3)\sum_i\sum_j U_{ij}a_i^*a_j^*$

Table 3. Selected Interatomic Distances (Å) and Angles (deg) for $Gd(Gd_6CoI_{12})$

		Distances	
Gd(2)−I(2)	3.1121(8)	Gd(1)−I(1)	3.0545(6)
Gd(2)−I(2)	3.1413(8)	Gd(2)−Gd(2)	3.7884(9)
Gd(2)−I(2)	3.3041(8)	Gd(2)−Gd(2)	3.7284(9)
Gd(2)−I(1)	3.1830(8)	Gd(2)−Co(1)	2.6577(5)
Gd(2)−I(1)	3.1927(8)		
		Angles	
I(1)−Gd(2)−I(2)	162.41(2)	Gd(1)−I(1)−Gd(2)	89.777(19)
I(1)−Gd(2)−I(2)	163.56(2)	Gd(1)−I(1)−Gd(2)	89.958(19)
I(1)−Gd(1)−I(1)	180	Gd(2)−I(1)−Gd(2)	72.91(2)
Gd(2)−Gd(2)−Gd(2)	59.466(9)	Gd(2)−I(2)−Gd(2)	73.20(2)
Gd(2)−Co−Gd(2)	180	Gd(2)−I(2)−Gd(2)	97.271(19)

The single-crystal structure of $Gd(Gd_6CoI_{12})$ was determined, and the data are presented in Tables 1−3. Unit cell parameters had been determined from Guinier camera powder diffraction film data,[16] but a single-crystal structure determination had not been reported. Since the powder diffraction data were obtained in the presence of a primary silicon standard, the smaller parameters found here (0.046 Å for a and 0.059 Å for c) are likely the result of drift in diffractometer angles between calibrations: the powder data were collected at ambient temperature, and the parameters would be expected to be longer.

The Gd_6Co trigonal antiprism is compressed along the c axis. This is manifest in the difference between the Gd(2)−Gd(2) distances within (3.7884(9) Å) and between (3.7284(9) Å) the triangular Gd_3 faces normal to the 3-fold axis. The average Gd(1)−Co distance is 0.038 Å longer than the corresponding Er−Co distance in $CsEr(Er_6CoI_{12})_2$[45] than in $Gd(Gd_6CoI_{12})$, a bit less than the difference in Shannon radii of Er and Gd (0.053 Å).[46]

The structure of $CsGd(Gd_6CoI_{12})_2$, shown in Figure 3, features Gd_6CoI_{12} clusters with 3-fold symmetry. This structure type is well described as an intergrowth of $Gd(Gd_6CoI_{12})$ and $Cs(Er_6CI_{12})$ structure types.[45] Because the clusters have C_3 symmetry, the 12 Gd−Gd edges are bridged by four crystallographically

(45) Submitted for publication.
(46) Shannon, R. D. *Acta Crystallogr.* **1976**, *A32*, 751−67.

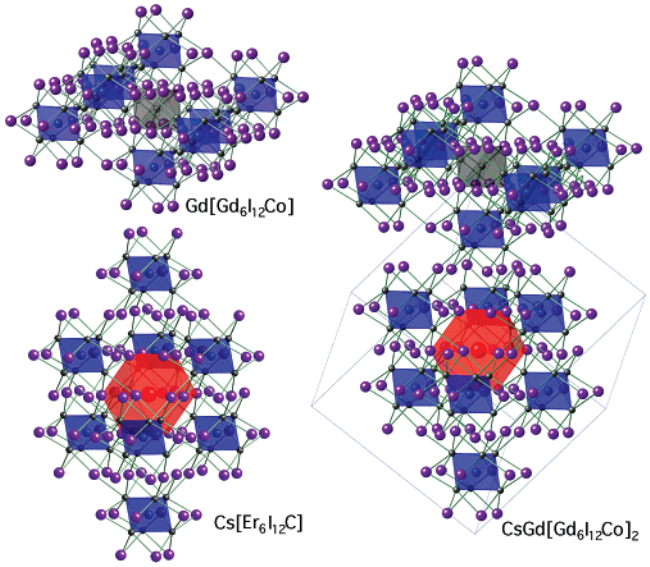

Figure 3. Structural relationship among $Gd[(Gd_6Co)I_{12}]$, $Cs[(Er_6C)I_{12}]$, and $CsGd[(Gd_6Co)I_{12}]_2$. The blue octahedra represent the Ln_6Z (Z = Co or C) units. The red cuboctahedron is a CsI_{12} coordination polyhedron, and the $Gd^{III}I_6$ octahedron is gray.

distinct iodine atoms. If one looks down the 3-fold axis, the three iodine atoms on the top form exo bonds to neighboring clusters and the three on the bottom bind to the isolated Gd^{III}. Of the six iodine atoms the bridge Gd−Gd bonds around the waist, three form exo bonds to neighboring clusters, and the other three form part of the Cs^+ ions' cuboctahedral coordination spheres.

Electronic Structure. Compounds of the $R[R_6ZI_{12}]$ structure type have been made with a variety of interstitial elements (Z), including several of the transition metals of groups 7−11 and the main group atoms B, C, and N as well as C_2.[16,41−44] Interstitials are essential to the formation and stability of these clusters; formally, they provide electrons to the electron-deficient R_6 cage and engage in strong R−Z bonding that is undoubtedly much stronger than the R−R bonding. We will briefly review the bonding scheme for these clusters to place the magnetic results in context. Figure 4 shows a molecular orbital diagram

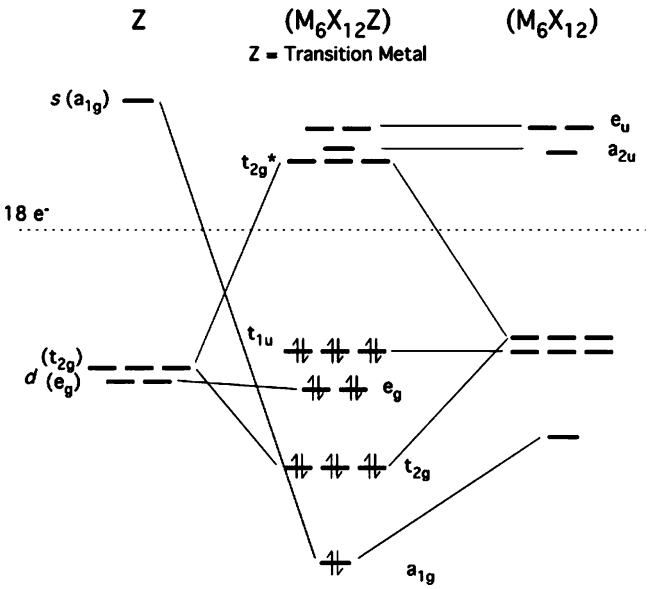

Figure 4. MO diagram of M_6X_{12} octahedral cluster with a transition metal element as the interstitial atom.

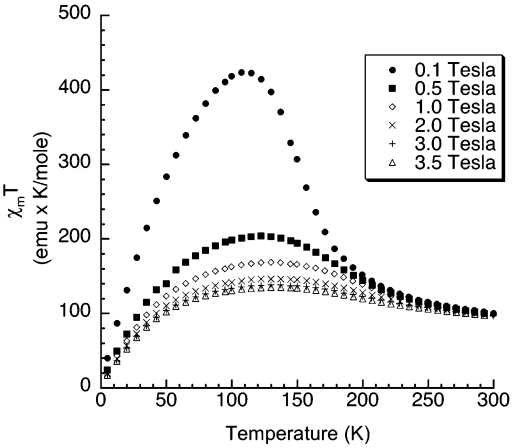

Figure 5. Ferromagnetic impurities in a sample of $Gd(Gd_6MnI_{12})$ are saturated by using larger applied fields. There is little difference between $\chi_m T$ at 3.0 and 3.5 T.

for the $[Gd_6ZX_{12}]$ clusters, where Z is a transition metal; levels that have predominately Gd 5d character are displayed. In O_h symmetry, first-row transition metal interstitial $t_{2g}/e_g(3d)$ and $a_{1g}(4s)$ orbitals interact with the cluster orbitals of like symmetry to form bonds with the surrounding Gd cluster. The highest occupied t_{1u} orbital, one of which is illustrated in **1**, is predominantly delocalized over the Gd_6 cage and is only slightly stabilized by a small contribution of Z-atom 4p orbitals. The electronic requirements for the Gd_6Z octahedron are given in Figure 4; a closed-shell cluster-based electron count of 18 applies.

The closed-shell configuration is achieved when Z = Co (i.e., the compound is $Gd[Gd_6CoI_{12}]$); the HOMO is fully occupied (t_{1u}^6). $[Gd_6FeI_{12}]^{3-}$ and $[Gd_6MnI_{12}]^{3-}$ clusters have t_{1u}^5 and t_{1u}^4 HOMO configurations, respectively.

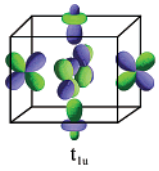

1

Magnetic Susceptibilities. Syntheses of these compounds are nearly quantitative, as indicated by powder diffraction measurements. Nevertheless, their magnetic properties are highly sensitive to the presence of ferromagnetic impurities, even in small proportions. All of the samples measured were at least to some extent contaminated with ferromagnetic impurities, and it was therefore necessary to measure magnetizations over a range of applied fields to determine the extent to which such impurities contribute. Figure 5 illustrates the saturation of ferromagnetic impurities by increasing the applied field. Data presented in Figure 6 are results obtained at an applied field of 3.5 T where saturation of the ferromagnetic impurities is virtually complete and was always verified by comparison with data at lower fields.

As indicated, the Gd_6Fe and Gd_6Mn clusters respectively possess one and two unpaired electrons, primarily delocalized over the six Gd atoms. In analyzing the susceptibilities of $Gd[Gd_6ZI_{12}]$ (Z = Mn, Fe, Co), we assume that the structurally isolated Gd^{III} center makes an ideal Curie-like Gd^{III} ($S = 7/2$) contribution that can be subtracted from the total susceptibility to obtain the susceptibility contribution, $\chi(Gd_6Z)$, made by the

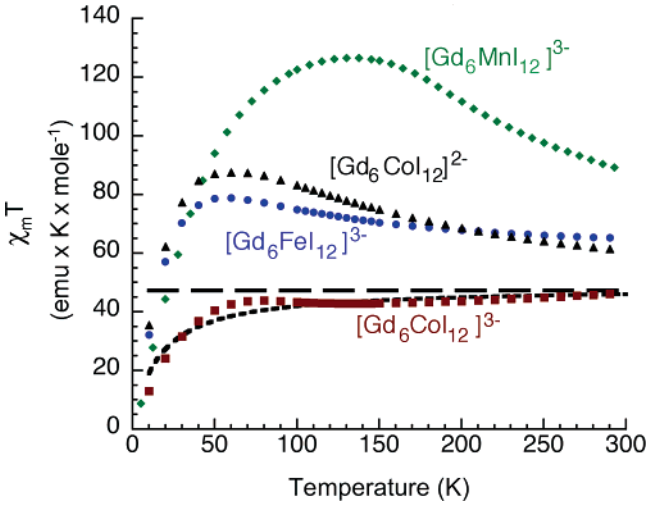

Figure 6. $\chi_m T$ vs T for $Gd(Gd_6CoI_{12})$, $Gd(Gd_6FeI_{12})$, $Gd(Gd_6MnI_{12})$, and $CsGd(Gd_6CoI_{12})_2$ at a 3.5 T applied field, adjusted according to eq 4. $\chi_m(Gd^{III})$ was subtracted from data for $CsGd(Gd_6CoI_{12})_2$, and the resultant was divided by 2 to yield a per cluster susceptibility for $[Gd_6CoI_{12}]^{2-}$. The Curie constant (47.25 emu K mol^{-1}) for an "ideal" cluster with six uncoupled Gd^{III} centers ($S = 7/2$; $g = 2$) is shown as the long-dashed line. The Curie−Weiss fit to $[Gd_6CoI_{12}]^{3-}$ is shown as the short-dashed line.

coupled cluster network:

$$\chi(Gd_6Z) = \chi - \chi(Gd^{III}) \qquad (4)$$

To help clarify the meaning of the magnetic data for these clusters, the data are plotted as $\chi_m(Gd_6Z)\cdot T$ vs T for the Mn-, Fe-, and Co-centered $Gd[Gd_6ZI_{12}]$ compounds in Figure 6.

As usual for this type of plot, ideal Curie law behavior results in a horizontal line wherein the intercept with the ordinate yields the Curie constant, C_m ($=\chi_m T$), that is related to the effective magnetic moment/cluster (μ_{eff}) via the relationship $C_m = (N_a\mu_B^2/3k_B)\mu_{eff}^2$. In Figure 6, a reference line is shown for the Curie constant expected for a collection of independent Gd spins ($J = S = {}^7/_2$ and taking $g_J = 2$): $C_m = 47.25$ emu K mol^{-1}. Deviations in $\chi_m T$ from the Curie line are an indication of the net effect of magnetic coupling as a function of temperature; values below (above) the Curie line indicate that the net alignment of moments with the external field is less (more) than expected for a collection of independent moments.

With a susceptibility approaching Curie behavior above 100 K, Gd_6CoI_{12} exhibits the weakest Gd−Gd exchange coupling among compounds in this series (though much larger in magnitude than normally observed for closed 5d-shell Gd^{III} compounds, where exchange coupling constants (J) are typically ~0.01 cm^{-1}). The Curie constant (C_m) obtained by fitting all the $\chi_m(Gd_6Co)$ data with a Curie−Weiss expression ($\chi_\mu = C_m/(T - \Theta)$) is 48.38 (±0.67) emu K mol^{-1}, and the Weiss constant (Θ) is −15.48 (±1.59) K.

Magnetism: Interpretation and Computational Results. The effective magnetic moment/cluster is increased considerably for the $[Gd_6FeI_{12}]^{3-}$ and $[Gd_6MnI_{12}]^{3-}$ systems in comparison with the compound with Co-centered clusters. As we discuss more fully below, this is attributable to relatively strong exchange interactions between the unpaired electrons in the HOMO and the electrons in the 4f orbitals. Neither compound

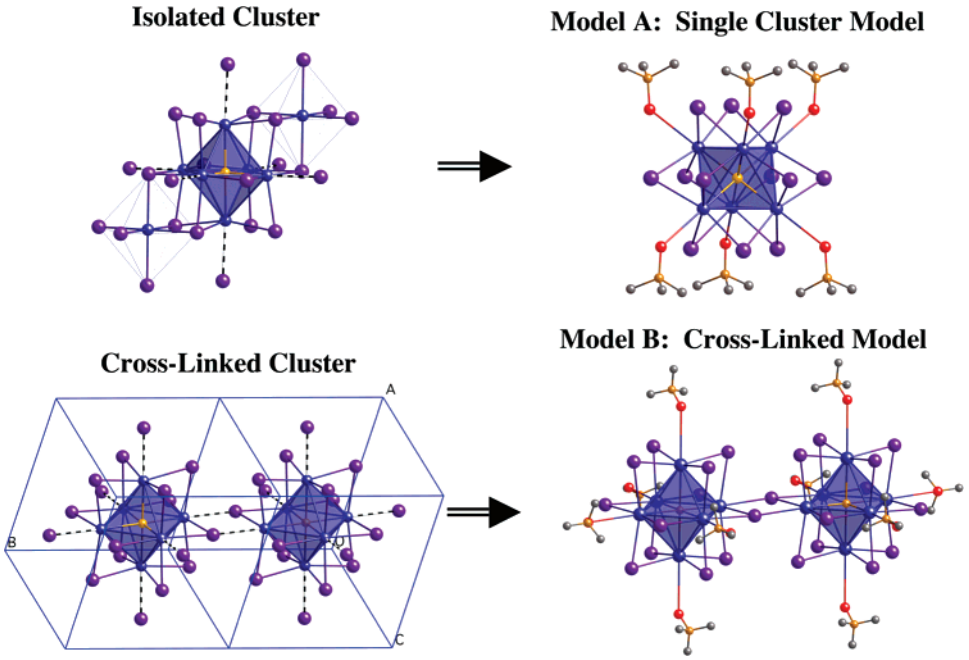

Figure 7. Relationship between the single cluster model (A) and cross-linked cluster model (B) and the parent $Gd[Gd_6ZI_{12}]$ structure.

yields a susceptibility that is well described by a Curie−Weiss fit, but it is clear that above 50 K the effects of ferromagnetic coupling dominate the data's departure from independent-moment behavior. The 16-electron $[Gd_6MnI_{12}]^{3-}$ cluster, having two holes in the HOMO, exhibits a significantly larger susceptibility over the entire measured temperature range than the 17-electron (one hole) $[Gd_6FeI_{12}]^{3-}$ system. All of these systems show the effects of substantial antiferromagnetic coupling at the lowest temperatures.

The clusters in $CsGd(Gd_6CoI_{12})_2$ possess 17 electrons for metal−metal bonding, and this compound therefore offers a useful control for our implicit hypothesis concerning the influence of open-5d-shell character on the magnetic properties of these compounds. Although these clusters are Co-centered, the cluster charge is 2−, so they are isoelectronic with the Fe-centered clusters in $Gd(Gd_6FeI_{12})$, which have a cluster charge of 3−. Figure 6 shows that the susceptibilities for the isoelectronic systems are indeed similar.

When there is only one hole in the HOMO as with the Fe-centered cluster, a break in the degeneracy of the three orbitals may cause incomplete delocalization of the hole. This could explain why we observe an effective magnetic moment lower than expected for complete ferromagnetic coupling (but see discussion below). With the 16-electron case, $Gd(Gd_6MnI_{12})$, having two holes in the HOMO, there is a larger magnetic moment/cluster but still not as large as expected for a $S = 44/2$ cluster.

As indicated in our earlier qualitative remarks, we attribute the strong intracluster coupling to the presence of appreciable unpaired spin density in metal−metal bonding electrons that are delocalized over the six metal atoms of the cluster. The clusters in these compounds are not structurally isolated, and hence, we should also expect intercluster coupling to exert an important effect on these compounds' magnetic properties. Nevertheless, it is instructive to first turn our attention to the stronger *intra*cluster magnetic coupling in clusters of this type. We investigated the model $[Gd_6CoI_{12}](OPH_3)_6$ as shown in Figure 7 (labeled model A) using DFT.

The model retains the $[Gd_6FeI_{12}]^{3-}$ cluster core structure but possesses a half-filled t_{1u}^3 HOMO configuration. The use of a half-filled t_{1u} subshell allows us to avoid computational complications that arise when one attempts to obtain a converged density when orbital degeneracy applies.[47] Phosphine oxide ligands fill the coordination sites provided by the Gd−I contacts lost upon separating the clusters, and they avoid unphysical charge density accumulation one obtains when anionic capping ligands are used. These ligands are also a logical choice from a synthetic point of view since they readily coordinate to rare earth atoms and have been used as capping ligands for $[Zr_6BCl_{12}]^+$ clusters.[48,49] A model system in which two clusters are cross-linked was constructed in the same spirit as the single-cluster model, and results from calculations should provide an estimate for the magnitude of the *inter*molecular interactions that occur in the solid state (model B in Figure 7). The two-cluster model maintains the clusters' solid-state structure, and phosphine oxide ligands again serve as terminating ligands. Partial geometry optimizations for the positions of the phosphine oxides were performed using an analogous yttrium model systems, $[Y_6CoI_{12}](OPH_3)_6$ and $[Y_6CoI_{12}]_2(OPH_3)_{10}$, resulting in structures with D_{3d} and C_i symmetries, respectively.

In calculations probing the manner in which the unpaired CBEs mediate the coupling of the $4f^7$ moments, we shall focus our attention on the ground CBE state, $^4A_{1u}$, from the t_{1u}^3 configuration. We carried out electronic structure calculations for 20 competing spin patterns on the single cluster model but shall first focus our attention on the cases where the three (5d character) electrons in the HOMO are all spin-up (i.e., $S = M_S$

(47) Calculations on a 17 CBE system, with a t_{1u}^5 configuration, resulted in different orbitals being occupied for the high-spin and broken-symmetry solution.
(48) Bradley, D. C.; Ghotra, J. S.; Hart, F. A.; Hursthouse, M. B.; Raithby, P. R. *J. Chem. Soc., Dalton Trans.* **1977**, 1166−72.
(49) Xie, X.; Reibenspies, J. H.; Hughbanks, T. *J. Am. Chem. Soc.* **1998**, *120*, 11391−400.

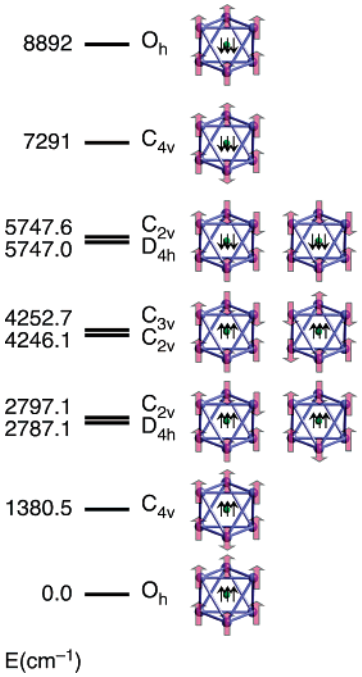

Figure 8. Ten spin patterns and energies for the model $[Gd_6CoI_{12}](OPH_3)_6$.

= 3/2). The calculated energies for those 10 patterns are shown in Figure 8.[50] In each case, we also indicate the symmetry of the potential that the 4f spin patterns impose on the valence electrons. Since the DFT calculations underestimate the magnitude of the $4f^7-5d$ exchange interaction for the Gd atom by ~11% (see ref 39) and because the exchange interactions in these molecular cases arise from essentially the same intraatomic $4f^7-5d$ exchange interaction, it is reasonable to assume that the spin pattern energy differences calculated here are underestimated by a similar margin.

The results from single cluster calculations indicate a remarkably strong preference for ferromagnetic coupling within the cluster. The lowest energy calculated spin pattern is that with all of the 4f spins aligned parallel to the spins of the three valence CBEs, the latter of which are spin-up in all calculations. Figure 8 shows that if the Gd 4f moments are successively "flipped" over, the energy increases in steps of ~1480 cm^{-1} (range: 1380−1600 cm^{-1}) for each Gd moment flipped. The spatial relationship between flipped moments has little direct effect; energy differences between *cis* and *trans* (C_{2v} and D_{4h}) or between *fac* and *mer* (C_{3v} and C_{2v}) spin patterns differ by less than 10 cm^{-1}.

A few comments concerning both the meaning of what we call "spin patterns" in the foregoing discussion and concerning the spin patterns not yet discussed are in order. First, we note that *only* the lowest energy spin pattern (all spins up) corresponds to a spin eigenfunction, and therefore all the other patterns have only semiquantitative significance. Second, spin patterns with two up-spin and one down-spin CBEs ($M_S = 1/2$) are primarily (though not entirely) derived from the doublet excited states of the cluster t_{1u}^3 CBE configuration (^2E_u, $^2T_{2u}$, and $^2T_{1u}$) that, when coupled to the $4f^7$ moments, yield energies that are interspersed with and bracketed by those listed in Figure 8 (the lowest at 3975 cm^{-1}; see Supporting Information). DFT

(50) A table depicting energies for all competing spin patterns is in the Supporting Information.

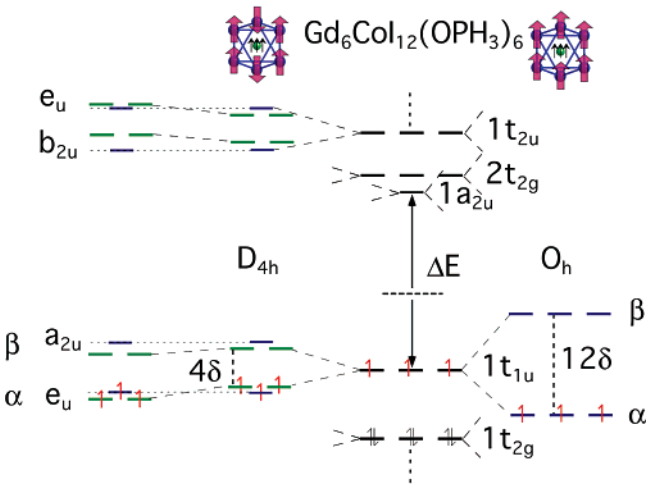

Figure 9. Perturbative analysis of d-electron-mediated f−f exchange for $Gd_6I_{12}Co(OPH_3)_6$: (far right) (de)stabilization and splitting of the α (*β*) orbitals for the O_h cluster induced by the exchange perturbation of all up-spin 4f moments; (left and far left) first- and second-order effects, respectively, of the 4f exchange field when two *trans*-4f moments are spin down (D_{4h} spin potential).

calculations enable us to estimate the range of the CBE state splittings to be ≲4000 cm^{-1} (see Supporting Information), and the magnitude of the $5d-4f^7$ coupling for the doublet cluster states is less than for the $^4A_{1u}$ state—which explains why the energies derived for the coupled doublet−$4f^7$ spin patterns interleave the coupled quartet−$4f^7$ spin patterns.

We have previously demonstrated the effectiveness of using a perturbative molecular orbital (PMO) model which describes the perturbation that the $4f^7$ exchange field exerts on electrons in molecular orbitals with 5d and 6s character to interpret 5d/6s-electron-mediated f−f exchange.[32,39,40] We apply this approach to the model compound $Gd_6CoI_{12}(OPH_3)_6$ and turn our attention to the cluster MOs shown in Figure 9. In our analysis, we compare two cases: the potential exerted by the six Gd $4f^7$ moments possesses O_h symmetry (the all 4f moments aligned) and the flipping of two *trans*-$4f^7$ moments imposes a spin-dependent D_{4h} symmetry potential on the valence electrons. Orbital plots clearly demonstrate that the d electrons reside in a delocalized t_{1u} orbital.[51] The $4f^7$ moment ordering induces a first-order splitting of the α- and *β*-spin molecular orbitals, but no symmetry breaking occurs since the exchange potential maintains symmetry. For the t_{1u}^3 configuration, the first-order splitting induced by the exchange perturbation yields a maximum possible stabilization. (Second-order effects are much smaller since only the energetically distant cluster orbital of t_{1u} symmetry can mix with the HOMO to "rehybridize" it.) First-order effects on the D_{4h} cluster will also stabilize the CBEs in the HOMO but to a lesser extent since those electrons tend to avoid the gadolinium atoms with opposed-spin 4f moments. The exchange perturbation lowers the symmetry and some mixing between the bonding and antibonding MOs is induced, yielding a second-order stabilization of both the α and *β* spin-orbitals. These second-order effects become significant only for an electron count where the HOMO is fully occupied, t_{1u}^6, which corresponds to the situation for $Gd(Gd_6CoI_{12})$.

One can construct a simple coupling model to account for the calculated relative energies of the spin patterns (Table 4).

(51) Molecular orbital plots are submitted as Supporting Information.

Table 4. Possible Equations Used in Calculating Heisenberg Coupling Constants (J's)*

$\Delta E_{A\text{-}S=45/2}$	$\sum_{i,j} z_{ij} J_{ij}$	DFT energy diff (cm^{-1})	Heisenberg energy diff (cm^{-1})
$\Delta E_{S=31/2-S=45/2}$	$2J_1$	1380.5	1448.6
$\Delta E_{S=17/2(D_{4h})\text{-}S=45/2}$	$4J_1$	2787.1	2897.2
$\Delta E_{S=17/2(C_{2v})\text{-}S=45/2}$	$4J_1$	2797.1	2897.2
$\Delta E_{S=3/2(C_{2v})\text{-}S=45/2}$	$6J_1$	4246.4	4345.8
$\Delta E_{S=3/2(C_{3v})\text{-}S=45/2}$	$6J_1$	4252.7	4345.8
$\Delta E_{S=11/2(D_{4h})\text{-}S=45/2}$	$8J_1$	5747.0	5794.4
$\Delta E_{S=11/2(C_{2v})\text{-}S=45/2}$	$8J_1$	5747.6	5794.4
$\Delta E_{S=25/2-S=45/2}$	$10J_1$	7291.1	7243.0
$\Delta E_{S=39/2-S=45/2}$	$12J_1$	8892.0	8691.6

Given that energy differences between 10 spin patterns is almost wholly dependent on the number of flipped $4f^7$ moments and not their stereochemistry, we can evaluate the exchange coupling constants by assuming that the Gd moments communicate solely through the Co interstitial atom with a single J value of +137.96 (0.93) cm^{-1}. The Hamiltonian associated with this calculated J value is simple:

$$\hat{H} = -J\sum_{i=1}^{6} S_{Gd}S_{Co} \qquad S_{Gd} = \frac{7}{2}; \qquad S_{Co} = \frac{3}{2} \qquad (5)$$

This reproduces the trends from the calculated energies and yields strong ferromagnetic coupling between the Gd centers through the Co "bridge" (**2**), but it is not to be taken very seriously insofar as the "Co" is concerned. The delocalized unpaired t_{1u} electrons, to which the cobalt 4p orbitals make a modest contribution, play the "Co" role.

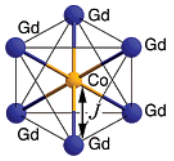

2

Our perturbative picture leads one to expect the energy difference between the high-symmetry state ($S = 45/2$) and the next lowest state ($S = 31/2$) to be approximately half the energy difference between the ^9D and ^7D states of the Gd atom,[39] assuming that the three metal−metal bonding electrons will share their time between six Gd atoms. Instead, the energy difference is approximately 25% of the $^9D-^7D$ difference. Several factors contribute to this "discrepancy". First, the CBEs are delocalized over the cluster, but the Co interstitial atom does contribute some 4p spin density in the HOMO (see Mulliken populations in Table 5). The extent to which electron density delocalized away from the Gd 5d orbitals into the Co 4p orbital decreases the 4f/5d exchange. The symmetry breaking patterns all induce greater spin polarizations, and the Co 4p contribution to the HOMO enables the electrons to avoid the opposed-spin Gd atoms to some extent. Second, the Gd 6s character also reduces the coupling because the 6s/4f exchange is ~75% smaller than the 5d−4f exchange. The Gd 6s character also increases in the t_{1u}-type orbitals for successively higher energy spin patterns.

To estimate the magnitude of *inter*cluster coupling, we performed two calculations using the model $(Gd_6CoI_{12})_2(OPH_3)_{10}$, which maintains the intercluster bonding found in the solid-state compound. Since the difference between the ferromagnetically coupled single cluster and the next lowest spin state was ~1400 cm^{-1}, we only considered the cross-linked models that contain *intra*cluster ferromagnetic coupling, assuming all other configurations will be much higher in energy. Figure 10 illustrates the energy difference between $S = 45$ and $S = 0$ in our cross-linked cluster model, which is 50 times weaker than intracluster couplings.

Table 5. Magnitudes of Co 4p and Gd 5d and 6s Spin Populations with All Values Computed with Precision within ±0.002

spin pattern	P_{Co} 4p	$P_{Gd}(4f^7\uparrow)$[a] 5d	$P_{Gd}(4f^7\uparrow)$[a] 6s	$P_{Gd}(4f^7\downarrow)$ 5d	$P_{Gd}(4f^7\downarrow)$ 6s	rel energy (cm^{-1})
$S = 45/2$	0.495	0.468	0.087			0
$S = 31/2$	0.500	0.468	0.091	−0.197	−0.028	1380.5
$S = 17/2$, D_{4h}	0.506	0.468	0.095	−0.205	−0.026	2787.1
$S = 17/2$, C_{2v}	0.506	0.479	0.092	−0.191	−0.028	2797.1
$S = 3/2$, C_{2v}	0.514	0.468	0.099	−0.201	−0.029	4246.4
$S = 3/2$, C_{3v}	0.513	0.479	0.096	−0.186	−0.032	4252.7
$S = 11/2$, D_{4h}	0.522	−0.198	−0.033	0.470	0.103	5747.0
$S = 11/2$, C_{2v}	0.522	−0.197	−0.033	0.482	0.100	5747.6
$S = 25/2$	0.533	−0.194	−0.038	0.486	0.104	7291.1
$S = 39/2$	0.545	−0.194	−0.042			8892.0

[a] Positive spin populations have the same sign as their respective 4f moments.

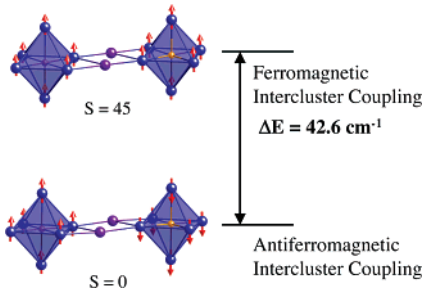

Figure 10. Energy difference between $S = 0$ and $S = 45$ for the cross-linked model.

The intercluster coupling favors antiferromagnetic spin alignment between clusters and an expected suppression of the susceptibility at low temperature. We calculate a magnetic coupling constant with a single J value; the associated Hamiltonian is

$$\hat{H} = -JS_{cluster1}S_{cluster2} \qquad S_{cluster1} = S_{cluster2} = \frac{45}{2} \qquad (6)$$

and the magnetic coupling constant is calculated to be −0.084 cm^{-1}.

We conclude with some notes of caution and explanation. The systems for which our computational models would be *most* appropriate do not yet exist. Data for a cluster compound with a t_{1u}^3 configuration are not reported in this paper, though research underway in our laboratory indicates that at least partial substitution of the Gd^{III} ion in $Gd(Gd_6MnI_{12})$, to yield $Ca_xGd_{1-x}(Gd_6MnI_{12})$, is synthetically feasible and that the resulting compound exhibits somewhat greater spin ferromagnetic coupling than even $Gd(Gd_6MnI_{12})$. Even more important is the fact that compounds with greater structural isolation of the Gd_6ZI_{12} cluster units are needed; in no system yet known are the clusters truly discrete. The Gd−I−Gd intercluster cross-linking is responsible for widening the HOMO-derived t_{1u} band to ~0.3 eV for both $Y(Y_6FeI_{12})$ and $CsY(Y_6CoI_{12})_2$ (in an extended Hückel calculation; see Supporting Information (struc-

ture adapted from the Gd congener)). The widening of this band weakens the otherwise very strong ferromagnetic coupling that we have predicted for a truly discrete $Gd_6ZI_{12}^{n-}$ cluster with a t_{1u}^3 configuration because the coupling is maximized for the $^4A_{1u}$ ground state. Achieving that state in a cross-linked solid requires that the t_{1u} electrons be unpaired over the entire band and entails an effective "promotion energy" cost.

Conclusions

Study of the homologous series of compounds $Gd(Gd_6ZI_{12})$ (Z = Co, Fe, Mn) demonstrates the efficacy with which unpaired, delocalized Gd−Gd bonding electrons can couple the spins localized in the 4f orbitals of the Gd atoms. Because of the strong exchange interactions between the electrons localized in the 4f orbitals in Gd and the valence (5d and 6s) electrons, strong magnetic communication can occur. The similarity in the temperature-dependent susceptibility of the isoelectronic compounds $Gd(Gd_6FeI_{12})$ and $CsGd(Gd_6CoI_{12})_2$ supports our contention that the magnetic properties of these compounds are largely dependent on the local electronic structure of the cluster and are less dependent on the structure of the extended network. Theoretical calculations on models of the clusters support the proposed exchange mechanism.

Gd_7MnI_{12}, Gd_7FeI_{12}, and $CsGd(Gd_6CoI_{12})_2$ all showed larger temperature-dependent magnetic susceptibilities on a per cluster basis than Gd_7CoI_{12}, which has a closed-shell cluster HOMO. However the magnitude of the susceptibilities were not as large as expected for a complete coupling of the magnetic moments of all the Gd atoms in the cluster. The lower than ideal magnetic susceptibility may, in part, be due to incomplete delocalization of the hole in the cluster HOMO caused by a break in the degeneracy of these orbitals. DFT calculations suggest that intercluster magnetic coupling is also significant. Structural isolation of the clusters will help to decipher the contributions of intra- vs intercluster coupling and will pave the way to an interesting class of molecular magnets in compounds appropriately doped with lanthanide elements other than gadolinium.

Acknowledgment. We thank the Robert A. Welch Foundation for its support through Grant A-1132 and the Texas Advanced Research Program through Grant Grant 010366-0188-2001. We thank the National Science Foundation for the X-ray diffractometers and crystallographic computing systems in the X-ray Diffraction Laboratory at the Department of Chemistry, Texas A&M University (Grant CHE-9807975), and the SQUID magnetometer (Grant NSF-9974899). We thank the Laboratory for Molecular Simulation at Texas A&M University for computing time and other support. We also like to thank Dr. Carmela Magliocchi for her instruction in crystallography and magnetic measurements.

Supporting Information Available: Crystallographic data in CIF format for $Gd(Gd_6CoI_{12})$, discussion of the state energy differences derived from the t_{1u}^3 configuration, spin pattern energies for 20 competing spin patterns of $[Gd_6CoI_{12}](OPH_3)_6$, molecular orbital plots for D_{4h} and O_h models of $[Gd_6CoI_{12}](OPH_3)_6$, and DOS plot for $Y(Y_6FeI_{12})$ and $CsY(Y_6CoI_{12})_2$. This material is available free of charge via the Internet at http://pubs.acs.org.

JA0617690